

Negative resistance for colloids driven over two barriers in a microchannel

Urs Zimmermann,^{1,*} Hartmut Löwen,¹ Christian Kreuter,² Artur Erbe,³ Paul Leiderer,² and Frank Smallenburg¹

¹*Institut für Theoretische Physik II: Weiche Materie,
Heinrich-Heine-Universität Düsseldorf, D-40225 Düsseldorf, Germany*
²*Fachbereich Physik, Universität Konstanz, D-78457 Konstanz, Germany*
³*Institut für Ionenstrahlphysik und Materialforschung,
Helmholtz-Zentrum Dresden-Rossendorf, D-01328 Dresden, Germany*

(Dated: May 24, 2022)

Ohm’s law is one of the most central transport rules stating that the total resistance of sequential single resistances is additive. Here we test additivity of resistances in classical systems of interacting colloids driven over two energetic barriers in a microchannel, using real-space microscopy experiments, particle-resolved simulations, and dynamical density functional theory. If the barrier separation is comparable to the particle correlation length, the resistance is highly non-additive, such that the added resistance of the second barrier can be significantly higher or lower than that of the first. Surprisingly, for a barrier separation comparable to the particle interaction range, the second barrier can add a *negative* resistance, such that two identical barriers are easier to cross than a single one. We explain our results in terms of the structuring of particles trapped between the barriers.

One of the basic characteristics of any transport situation is the resistance, commonly known from electric circuits, which is in general defined as the ratio of the transport flux and the driving force, typically in the linear-response regime of small drives. For both electric circuits and classical transport, Ohm’s law states that when resistors are put in series, their resistances simply add up. However, this macroscopic law is expected to break down on the microscopic scale, in particular when the distance between the two obstacles approaches the correlation length of the transported particles.

Knowing and controlling flow resistance is of particular importance when tuning the transport of solutes through channels. This type of transport is the basic situation in microfluidics [1], where the transported objects are typically micron-sized colloidal solutes, such that thermal fluctuations play a significant role [2]. Moreover, there are many other examples where individual “particles” (or agents) are propagating through channels. Examples include macroscopic objects like cars or pedestrians [3], animals [4] and bacteria [5–7] migrating collectively through channels, and the transport of ions through membranes via nanopores [8]. Obstacles in such channels naturally inhibit the overall steady-state rate at which the particles are able to traverse the channel, providing an effective resistance to the flow. In channels with multiple obstacles, we expect Ohmic (i.e. additive) behavior of the corresponding resistances when the separation between the obstacles is large, and a breakdown of Ohm’s law for smaller distances. The crossover between these regimes is determined by the correlation length in the system, i.e. the length scale associated with local structure in the fluid of transported particles. Detailed knowledge of these non-additive effects is of vital importance for the design of efficient microfluidic devices, as well as for our broader understanding of constricted flow phenomena.

In this Letter, we explore the additivity of resistances in mesoscopic colloidal suspensions driven through a microchannel [9]. We first perform an experiment on repulsive colloidal particles confined to microchannels containing two step-like barriers on the substrate, and measure the current through the channels as a function of the strength of the gravitational driving force. Subsequently, we employ Brownian dynamics simulations and dynamical density functional theory to systematically explore the interplay between the two barriers. Our results show strong deviations from additivity for the resistance of two barriers when the separation between the two obstacles is comparable to the correlation length of the system, which is on the order of several interparticle spacings. Amazingly, if the barrier separation is comparable to the interaction range, we discover that the resistance contributed by the second barrier can even be *negative*. We explain this counterintuitive effect of negative resistance via the long-ranged particle interactions and the ordering of the particles trapped between the two barriers. When these particles are disordered, they exhibit spontaneous fluctuations which modulate their interactions with particles crossing the barriers, significantly enhancing barrier crossing rates [10, 11]. This surprising phenomenon provides a route for tuning and enhancing particle flow over an obstacle by the inclusion of additional barriers, reminiscent of the use of geometric obstacles to assist e.g. the flow of panicked crowds [12].

In our experiment, colloidal superparamagnetic particles are confined in a microchannel with obstacles, prepared using molds made via microlithography [9, 13], see Fig. 1. The experimental cell consists of two rectangular reservoirs, connected by multiple channels (to improve statistics). The colloidal particles are restricted to two-dimensional in-plane motion due to gravity. In each channel up to two U-shaped step-like barrier structures are

implemented perpendicular to the channel, for details see Supplemental Material [14]. A uniform external magnetic field \mathbf{B}_{ext} is applied in the direction perpendicular to the plane in which the particles move. This magnetic field induces purely repulsive interactions between the colloidal particles.

We measure the particle current in the channel as a function of the gravitational driving force, controlled by the tilt angle of the setup, for channels with zero, one, and two barriers. In the absence of barriers, the current shows a trivial linear dependence on the driving force, shown by the blue line in Fig. 1d. For a single barrier (green line in Fig. 1d), we observe a crossover from a zero-flow regime at small driving forces (where the driving force is too weak to push particles across the barrier) to an approximately linear regime for large driving forces [9]. Hence, the barrier provides a resistance to the flow, which reduces the particle current. Adding a second barrier to a channel results in a clear non-additivity of the resistance of the two barriers. In particular, for two barriers separated by approximately 2.5 times the typical interparticle distance (red line in Fig. 1), the second barrier has a much stronger effect on the total particle current than the first one, indicating a higher effective resistance.

To explore this non-additivity in detail, we make use of overdamped Brownian dynamics simulations and dynamical density functional theory (DDFT) calculations. We consider a two-dimensional system with periodic boundary conditions along the channel (x -direction), containing N particles interacting via a dipolar repulsion

$$\beta V_{\text{int}}(r) = \Gamma \left(\frac{a}{r}\right)^3, \quad (1)$$

where $\beta = 1/k_B T$ with k_B Boltzmann's constant and T the temperature, Γ is the dimensionless interaction strength, and $a = \rho_0^{-1/2}$ sets the length scale of a typical interparticle spacing of a given mean number density ρ_0 . The particles additionally experience a constant driving force $F\hat{x}$ pushing the particles along the channel.

The confining channel and barriers are modeled as an external potential $V_{\text{ext}}(x, y) = V_{\text{channel}}(y) + V_{\text{barrier}}(x)$. The first term here is a steep repulsive wall potential confining the particles in one direction. V_{barrier} represents one or two parabola-shaped potential barriers with width a and height $V_0 = 10 k_B T$, see Fig. 2b inset and Supplemental Material [14]. We choose the channel width $L_y = 4.65a$, and the channel length L_x such that the total number density $\rho_0 = N/(L_x L_y) = 1/a^2$ for a given particle number N .

In our DDFT calculations [15, 16], we choose the Ramakrishnan–Yussouff functional [17] to model interacting particles in a fluid state ($\Gamma = 5$). In addition to DDFT, we perform Brownian Dynamics simulations of particles experiencing the same potentials and external driving force. As a reference we provide an analytical

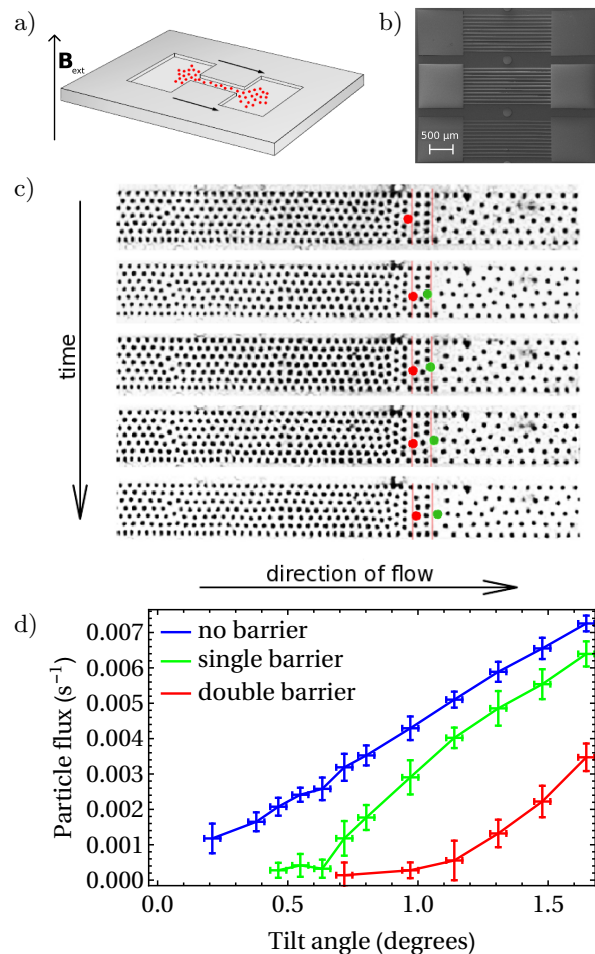


FIG. 1. a) Schematic setup of the experiment: two particle reservoirs are connected by a microfluidic channel through which particles are flowing due to gravity. b) Top view of the experimental system. c) Snapshots of a two barrier system for different times. The position of the barriers is indicated by a red vertical line. Two particles are highlighted in red and green. d) Flux as a function of tilt angle in a system with no barriers (blue line), single barrier (green line) and double barriers (red line). The initial density was $\rho_0 = (7.23 \pm 0.5) \times 10^{-3} \mu\text{m}^{-2}$, and the external field strength was 0.6 mT. The separation between the two barriers was $30 \mu\text{m}$.

solution for non-interacting particles ($\Gamma = 0$). See Supplemental Material [14] for details.

Using both DDFT and simulations, we explore the relation between the total steady-state particle current J along the channel, the driving force F on the particles, and the distance Δx between the two barriers. The ratio of the driving force and current characterizes the total resistance of the system, $R^{\text{tot}} = \frac{F}{J}$. In a channel without barriers, the particles trivially adopt the average drift current $J_0 = F \rho_0 L_y \xi^{-1}$, where ξ is the friction coefficient of the background solvent, leading to an inherent background resistance $R_{\text{bg}} = \xi / (L_y \rho_0)$. In a single-barrier system, the resistance R_1 added by the barrier can be

extracted from the total resistance $R_s^{\text{tot}} = R_{\text{bg}} + R_1$ by measuring the single-barrier current J_s :

$$R_1 = R_s^{\text{tot}} - R_{\text{bg}} = F \left(\frac{1}{J_s} - \frac{1}{J_0} \right). \quad (2)$$

Similarly, in a double-barrier system (with current J_d), the total resistance is $R_d^{\text{tot}} = R_{\text{bg}} + R_1 + R_2$, and the effective resistance of the second barrier R_2 can be written as

$$R_2 = F \left(\frac{1}{J_d} - \frac{1}{J_s} \right). \quad (3)$$

In the case of additivity, the resistance R_2 of the second barrier will be equal to R_1 (the resistance of the first barrier), while deviations from this rule will indicate non-additivity.

In Fig. 2, we plot R_2/R_1 for a range of barrier separations Δx at different driving forces F , as obtained from analytical theory [14] (a), DDFT calculations (b), and computer simulations (c). For non-interacting particles R_2 is lowest when the two barriers are touching ($\Delta x = a$) and converges exponentially to R_1 for larger distances. In contrast, for interacting particles and for all investigated F , the resistance of the second barrier is highest at $\Delta x = a$. At this separation the resistance added by the second barrier can be many times higher than R_1 , signaling strong non-additivity. More interestingly, for slightly larger separations ($\Delta x \simeq 1.5a$), R_2 becomes smaller than R_1 , and even negative for sufficiently weak driving forces. In this regime, the addition of the second barrier *reduces* the overall resistance in the channel. At larger Δx , R_2 shows decaying oscillations, converging towards the additive case ($R_2 = R_1$), as expected at sufficiently large distances.

We can understand this observation by considering the interactions between the particles. Since these are dipolar in nature, they are sufficiently long-ranged to span across the barrier. Hence, a particle on top of the barrier experiences forces from particles between the two barriers, which depend on the density and structuring of those particles. In Fig. 3 we plot the density profile of the particles $\rho_x(x)$, projected onto the long axis of the channel, for various barrier separations Δx , as well as for a single barrier. In the single-barrier case, we always observe a high density peak in front of the barrier, and a slightly lower peak just after the barrier (see Fig. 3a). In the two-barrier cases, the additional peaks in between the two barriers vary in height based on Δx . For very small separations (Fig. 3b), where the resistance of the second barrier is high ($R_2 > R_1$), we find a single sharp density peak between the barriers, which is significantly higher than the peak observed after a single barrier. Here, particles between the barriers are arranged in a single line with little room for fluctuations, and hence provide a strong and relatively constant force on particles crossing

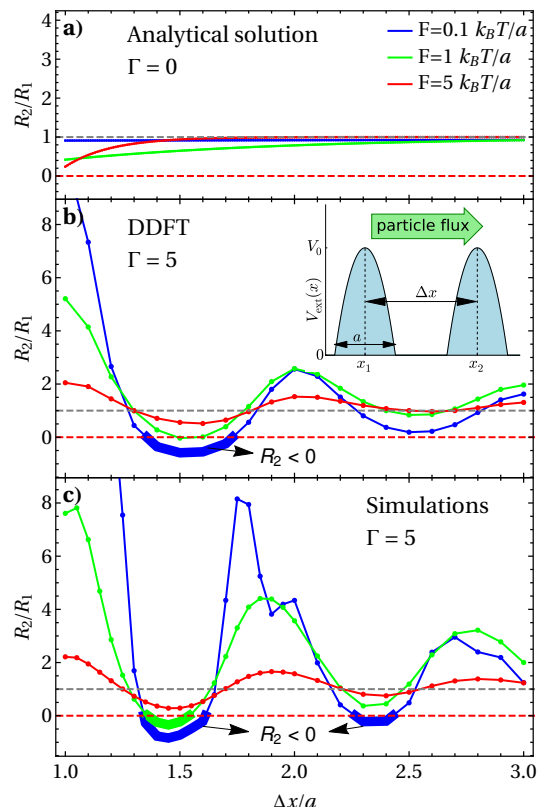


FIG. 2. (Color online) Effective resistance R_2 of the second barrier relative to the resistance R_1 of the first barrier, as a function of the barrier spacing Δx , at different driving forces. The dashed lines highlight special values of R_2 : the gray line shows Ohmic additivity and the red line marks the onset of negative effective resistance. Results are shown for analytical theory [14] at $\Gamma = 0$ (a), DDFT at $\Gamma = 5$ (b), and simulations at $\Gamma = 5$ (c). A sketch of the barrier configuration is shown in inset b.

the first barrier, pushing them back. In the regime where $R_2 < R_1$ (Fig. 3c), we instead see two much lower peaks, indicating a structure with two layers and significantly larger fluctuations. These larger fluctuations not only provide space for particles entering via the first barrier, but also modulate the force exerted on particles crossing the barriers, resulting in a fluctuating effective barrier height. For weak driving forces, barrier crossings are rare events, whose rate depends exponentially on the barrier height. Fluctuations in barrier height are known to lead to significantly higher crossing rates [10, 11] and hence higher currents. Finally, for larger separations, where $R_2 > R_1$ again, we observe two higher peaks, indicating a more structured pair of layers between the barriers.

We confirm this intuitive picture by plotting in Fig. 4 the relative height of the first peak after the first barrier $\delta\rho^{\text{peak}} = \rho_d^{\text{peak}}/\rho_s^{\text{peak}}$, where ρ_s^{peak} is the height of the first peak after a single barrier, and ρ_d^{peak} is the height of the first peak after the first of two barriers. When plotted as a function of Δx , the peak height (blue in

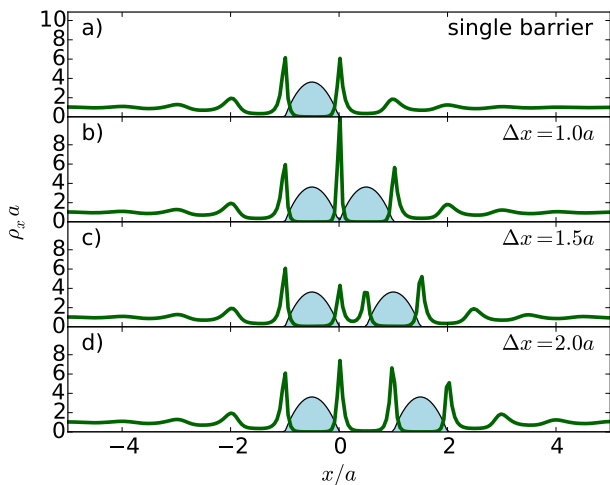


FIG. 3. Local density profiles as a function of distance along the channel at the same interaction strength ($\Gamma = 5$) and driving force $F = 0.1k_B T/a$, as obtained via DDFT. From top to bottom, we show a system with a single barrier, and systems with two barriers at separations $\Delta x/a = 1.0, 1.5$, and 2.0 .

Fig. 4) indeed strongly correlates with the particle current (red) in both the DDFT framework and the simulations. In our particle-resolved simulations, the additional fluctuations of the particles in between the two barriers are clearly visible. Moreover, examining simulation trajectories demonstrates that for most barrier separations, whenever a particle crosses the first barrier, the sudden increase in density between the barriers typically leads to the rapid expulsion of a particle over the second barrier. This observation confirms that the first of the two barriers can indeed be considered as the main bottleneck for the overall flow process. However, for $\Delta x \lesssim 1.3$, the bottleneck is instead the crossing of the *second* barrier. Here, particles form a single narrow layer between the two barriers, which inhibits the possibility of collectively pushing a particle across the second barrier. This may explain the reduced correlation between $\delta\rho_{\text{peak}}$ and R_2/R_1 for small Δx in Fig. 4.

In conclusion, we have explored the effect of sequential potential energy barriers on the flow of colloidal particles driven through microchannels. As our experiment shows, two barriers close together can result in drastically higher resistance than twice the resistance of a single barrier. Moreover, via a detailed investigation of this non-additivity using both simulations and dynamical density functional theory, we discover that depending on the barrier spacing, the second barrier can add an effective resistance that is higher than the resistance of a single barrier, lower, or even negative. In the negative regime, the presence of the second barrier helps particles cross the first barrier, contrary to what intuition would suggest. We show that this enhanced barrier-crossing rate can be attributed to the structuring of the layer of particles in be-

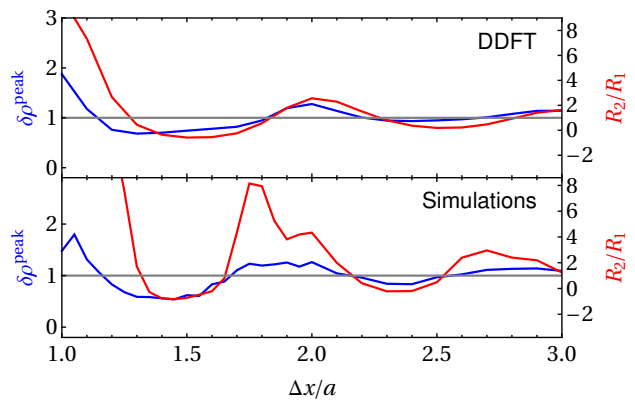


FIG. 4. Height of the first density peak after the first barrier (normalized by the height of the peak after a single barrier) as a function of barrier separation at fixed driving force $F = 0.1k_B T/a$ and interaction strength $\Gamma = 5$, as obtained from DDFT (top) and simulations (bottom).

tween the two barriers: weaker structuring (evidenced by lower peaks in the density profile) increase the current. A vital component for this phenomenon is the requirement that particles on top of the barriers can still interact with the particles aggregated just before and after that barrier, necessitating sufficiently long-ranged interactions. Indeed, preliminary simulations show a clear reduction of the observed non-additivity when the barrier is wider in comparison to the interaction range. As a second requirement, the density should be high enough to enable significant ordering of particles. In the confined region between the barriers, the ordering will depend sensitively on the ratio of the barrier spacing Δx and the preferred spacing between neighboring layers of particles, as long as Δx is small compared to the correlation length in the system. Similar confinement effects have shown to result in oscillatory behavior in forces between plates or spheres immersed in a background of smaller particles [18]. Interestingly, the effect of negative resistance is reminiscent of the interplay between reflecting barriers in quantum-mechanical systems, where interference is known to lead to enhanced transmission for certain barrier spacings, as used in e.g. Fabry-Perot interferometers [19].

The sensitivity of the resistance to the barrier separation and microscopic particle interactions provide a method to tailor and control flow through channels [20–22] or porous media [23]. Interestingly, *geometric* obstacles have similarly been shown to enhance flow [24], as applied in e.g. the design of emergency exits [12, 25]. However, in these cases, enhanced flow rate is typically observed when the added obstacle is placed *before* the bottleneck, rather than behind it.

The possibility of mitigating a flow-resisting barrier by placing another barrier behind it might have important implications in microfluidic devices. Moreover, the specificity of this approach to relatively long-ranged interac-

tions suggests an opportunity for separating different particle species, or enhanced flow control via external fields modifying the interactions. Further applications include the directed transport of strongly charged dust particles in a plasma [26] and congestions in granulates [27], as well as jammed flow situations of colloids [28], or agents through constrictions [29]. In particular, a jammed situation near an obstacle may be avoided by adding further obstacles. An interesting question for future research is whether the effective total resistance could be further tuned by using a combination of three, four, or an infinite number of obstacles [30] (forming e.g. a ratchet [31, 32]), or by using barriers of differing heights.

We gratefully acknowledge funding from the German Research Foundation (DFG) within project LO 418/19-1. We thank Arjun Yodh, Laura Filion, and Marco Heinen for helpful discussions.

* urs.zimmermann@uni-duesseldorf.de

- [1] T. M. Squires and S. R. Quake, *Rev. Mod. Phys.* **77**, 977 (2005).
- [2] P. Hänggi, P. Talkner, and M. Borkovec, *Rev. Mod. Phys.* **62**, 251 (1990).
- [3] D. Helbing, *Rev. Mod. Phys.* **73**, 1067 (2001).
- [4] D. J. T. Sumpter, *Phil. Trans. R. Soc. B* **361**, 5 (2006).
- [5] M. B. Wan, C. J. Olson Reichhardt, Z. Nussinov, and C. Reichhardt, *Phys. Rev. Lett.* **101**, 018102 (2008).
- [6] H. H. Wensink, J. Dunkel, S. Heidenreich, K. Drescher, R. E. Goldstein, H. Löwen, and J. M. Yeomans, *Proc. Natl. Acad. Sci. USA* **109**, 14308 (2012).
- [7] H. H. Wensink and H. Löwen, *Phys. Rev. E* **78**, 031409 (2008).
- [8] J. Dzubiella and J.-P. Hansen, *J. Chem. Phys.* **122**, 234706 (2005).
- [9] C. Kreuter, U. Siems, P. Henseler, P. Nielaba, P. Leiderer, and A. Erbe, *J. Phys.: Condens. Matter* **24**, 464120 (2012).
- [10] D. L. Stein, R. G. Palmer, J. L. Van Hemmen, and C. R. Doering, *Phys. Lett. A* **136**, 353 (1989).
- [11] P. Pechukas and P. Hänggi, *Phys. Rev. Lett.* **73**, 2772 (1994).
- [12] N. Shiwakoti and M. Sarvi, *Transp. Res. Part C: Emerg. Technol.* **37**, 260 (2013).
- [13] J. R. Anderson, D. T. Chiu, H. Wu, O. J. Schueller, and G. M. Whitesides, *Electrophoresis* **21**, 27 (2000).
- [14] See Supplemental Material at xxx for additional details on the experimental setup, model, DDFT calculations, analytic theory, and simulations.
- [15] U. M. B. Marconi and P. Tarazona, *J. Chem. Phys.* **110**, 8032 (1999).
- [16] A. J. Archer and R. Evans, *J. Chem. Phys.* **121**, 4246 (2004).
- [17] T. V. Ramakrishnan and M. Yussouff, *Phys. Rev. B* **19**, 2775 (1979).
- [18] R. Roth, R. Evans, and S. Dietrich, *Phys. Rev. E* **62**, 5360 (2000).
- [19] M. Vaughan, *The Fabry-Perot Interferometer: History, Theory, Practice and Applications, Series in Optics and Optoelectronics* (Taylor & Francis, New York (USA), 1989).
- [20] B. Lindner and L. Schimansky-Geier, *Phys. Rev. Lett.* **89**, 230602 (2002).
- [21] R. Gernert and S. H. L. Klapp, *Phys. Rev. E* **92**, 022132 (2015).
- [22] M. F. Carusela and J. M. Rub, *J. Chem. Phys.* **146**, 184901 (2017).
- [23] M. Spanner, F. Höfling, S. C. Kapfer, K. R. Mecke, G. E. Schröder-Turk, and T. Franosch, *Phys. Rev. Lett.* **116**, 060601 (2016).
- [24] F. Alonso-Marroquin, S. I. Azeezullah, S. A. Galindo-Torres, and L. M. Olsen-Kettle, *Phys. Rev. E* **85**, 020301 (2012).
- [25] J. Tanimoto, A. Hagishima, and Y. Tanaka, *Physica A* **389**, 5611 (2010).
- [26] G. E. Morfill and A. V. Ivlev, *Rev. Mod. Phys.* **81**, 1353 (2009).
- [27] I. Zuriguel, A. Garcimartín, D. Maza, L. A. Pugnaloni, and J. M. Pastor, *Phys. Rev. E* **71**, 051303 (2005).
- [28] P. Kanehl and H. Stark, *Phys. Rev. Lett.* **119**, 018002 (2017).
- [29] A. J. Liu and S. R. Nagel, *Nature* **396**, 21 (1998).
- [30] U. Siems and P. Nielaba, *Phys. Rev. E* **91**, 022313 (2015).
- [31] P. Hänggi, F. Marchesoni, and F. Nori, *Ann. Phys.* **14**, 51 (2005).
- [32] M. Evstigneev, S. von Gehlen, and P. Reimann, *Phys. Rev. E* **79**, 011116 (2009).